Measuring deflection of the vertical via local reference point surveying and pointing calibration of VLBI telescope: a case study at Urumqi station

Zhibin Zhang[1,2], Xiaohui Ma[3], Zhongmiao Sun[3], Ali Zhang[4], Ye Yuan[4], Zhengxiong Sun[1]

[1]Shanghai Astronomical Observatory, Chinese Academy of Sciences, Shanghai 200030, China
[2]University of Chinese Academy of Sciences, Beijing 100049, China
[3]Xi'an Research Institute of Surveying and Mapping, Xi'an 710054, China
[4]Xinjiang Astronomical Observatory, Chinese Academy of Sciences, Urumqi 830011, China

Key Points:

- Propose two new non-optical methods to determine the DOV of VLBI telescope.
- Give the generalized expression of pointing calibration model regarding of axis related errors.
- Establish the connections among VLBI delay observing, reference point determination and telescope pointing calibration.

Corresponding author: Zhibin Zhang, zbzhang@shao.ac.cn

Abstract

Deflection of the Vertical (DOV) is vital to astro-geodetic and geophysics research and application. In the Urumqi station, two new non-optical methods including small network coordinate transformation (SNCT) and azimuth-axis inclination inversion (AAII),are proposed to determine the DOV of the VLBI telescope. The generalized expression of the pointing calibration (PC) model regarding of axis related errors is also presented. Therefore, the PC model and indirect model (IM) used for reference point determination (RPD) are unified by redefining their coordinate system, angle direction, axis related errors. The DOV result of the SNCT method has good agreement with those DOVs solved by the real surveying and other different models, e.g., early Global Navigation Satellite System (GNSS) and leveling measurements (EGL), mass integration model(MIM), etc.. Due to the possible asymmetric coverage of calibrating sources in the north-south direction in PC, the north-south DOV component of AAII varies in its value with the surveyed value. However, the west-east DOV component fits well in both direction and magnitude.

The proposed methods enable the VLBI telescope to sense the direction of the local plumb line via introducing local leveling. We also establish the connections among VLBI delay observing, RPD and telescope PC, which has a benefit to muti-tech systematic error identification, monitoring and correction. The research indicates that, similar to local surveying and VLBI observing, the telescope point calibration can be also taken as a regular technique to monitoring systematic error.

1 Introduction

Deflection of the Vertical (DOV), the angle at a given point on the Earth between the vertical and the direction of the normal to the reference ellipsoid through that point (Hermann and Bucksch , 2014) , is critical to different directions (Barzaghi et al. , 2016) in geodesy, e.g., the transformation between astronomical and geodetic results including coordinates and azimuth angles, the transformation between different height system, reduction of horizontal and vertical angles to an ellipsoid surface, geodetic net calculations and geoid detection, etc. The critical applications of DOV and its variation, i.e. the Plumb Line Variations (PLV) (Li et al. , 2001; Tanaka et al. , 2001; Li and Li , 2009), probably are national defense, aerospace and geophysics research. The latter reveals underground material migration, which has a significant impact on embodied earthquake signal analysis and could contribute to monitoring earthquakes. Both IAU and IAG pay much attention to studying in DOV.

The methods of DOV determination include astro- and geodetic observing, e.g. the observing equipments have updated from traditional astronomical theodolite or zenith tube to digital zenith telescope in recent years, which has an absolute axis pointing error of 1∼2" and 0.2" observing internal coincidence, respectively; early Global Navigation Satellite System (GNSS) and leveling measurements (EGL), e.g. 0.7" calculating accuracy could obtained using the geoid in an accuracy level of several cm, which is available for small and linear terrain area (Ceylan , 2009); gravitational methods, e.g. the mean accuracy of DOV in China gravitational field and quasi-geoid system (CGGM) 2000 could reach up to 1.5" (Sun et al. , 2005).

Very long baseline interferometry (VLBI) is a geometrical correlation timing technology based on extragalactic radio sources, which was born in 1965. Since it is the only technique that links the celestial reference system to the terrestrial reference system and Earth orientation parameters, regular global VLBI observation has been carried out close to half a century (Schuh and Behrend, 2012). Radio telescopes (or antennas) are necessary components of VLBI. In order to ensure the basic function of the telescope and obtain tie-vectors among different observing equipments, irregularly telescope *pointing*

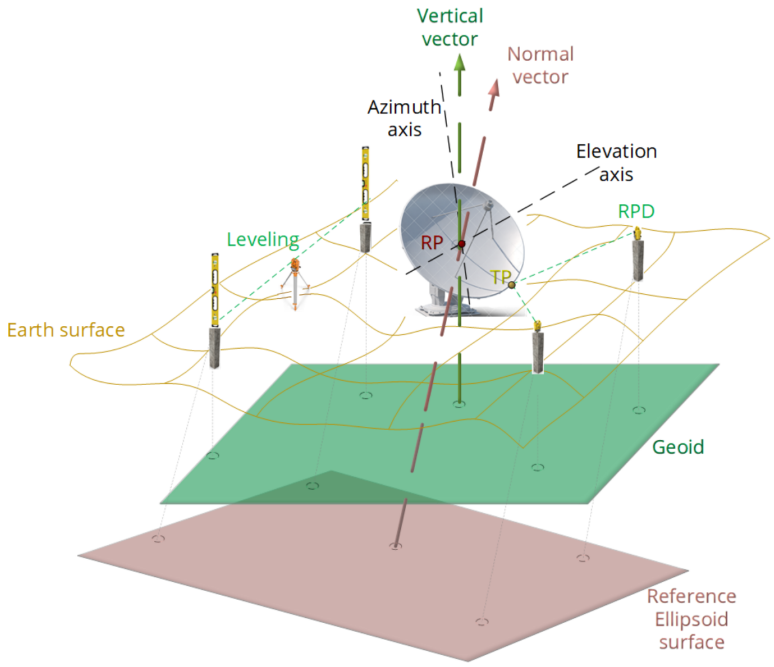

Figure 1. Schematic of the RP and DOV determination at a VLBI station

calibration (PC) and *reference point (RP) determination (RPD)* have been performed in different VLBI stations. However, the PC and RPD surveying have been mutually independent in VLBI stations. Besides, due to the insensitive of VLBI to feeling the gravity, VLBI station has to introduce the above mentioned methods to determine its DOV, e.g. using digital zenith telescope or GNSS and leveling. It is time-consuming to avoid cloudy or rainy day and daytime caused by the disadvantage of optical observing and also a heavy workload to transport the instruments. Therefore, few VLBI stations have directly determined DOV. In order to extend the function of VLBI station, contributing more DOV products to refine gravity field models and realizing a sustained DOV monitoring using widespread and long-term maintained VLBI stations, we consider that once the local leveling information imported, whether VLBI telescope could become sensitive to the gravity, then the DOV could be determined from local RPD surveying or inverted in telescope axis information.

Urumqi (or Nanshan) station of Xinjiang astronomical observatory is a VLBI-GNSS co-located station and plays an important role to maintain a global, especially for a Central Asia geodetic datum, where the main peaks of Tianshan mountain locates on its south side. Apparently, there must be a bigger DOV value and the station will be a good testing place for methods verification. Its *local control network (LCN)* to RPD covers within 170 m in square. Hence, we consider when the DOVs in such a small region are assumed to be equivalent, whether the DOV can be solved using only RPD and(or) PC data.

In this paper, in terms of used alt-azimuth mount telescope, we propose two new methods for determining the DOV of VLBI telescope in Sect. 2. Experiments, results and discussion are shown in Sect. 3. Conclusion remarks are given in Sect. 4.

2 Principle

Two methods named as *small network coordinate transformation (SNCT)* and an *azimuth-axis inclination inversion (AAII)* will be proposed to determine the DOV of the VLBI station in this section.

Once a VLBI telescope finished its construction, the RP coordinate of the telescope will be measured via local surveying based on GNSS frame. Besides, from then on, the vector(s) connecting the telescope RP and the RPs of other space-geodesy facilities around the telescope, e.g. GNSS antenna, will also be determined irregularly. The local surveying period of the VLBI global observing system (VGOS) stations is recommended as ∼2.5 yr (Petrachenko et al., 2009).

As shown in Fig. 1, some pillars were constructed around a VLBI telescope and they constitute a LCN to determine the RP of the telescope. Generally, the RPD surveying includes 3 steps:

Step 1: GNSS synchronous loop observing and local ground leveling on these pillars to obtain the coordinates include height datum of the LCN. The precision of the coordinates of these marks on the pillars can reach up to the level of sub-millimeter ;

Step 2: scattered target trace points (TPs) surveying based on e.g. a total station and the pillars in LCN. The targets are fixed on and followed-up with the different orientations of the telescope to form the scattered TPs.

Step 3: solving RP using TPs and telescope pointing information via some indirect methods.

It is noteworthy that leveling instrument and TP surveying instrument, e.g. a total station, should be leveled before ground leveling and TP observing. It indicates that the local plumb line is introduced via leveling.

2.1 The Principle of SNCT

If the DOV values at different points in a small region can be regard as equivalent within a certain range of accuracy, the DOV can be determined using the SNCT. The geocentric coordinates of the marks in LCN can be obtained after GNSS synchronous loop observing and adjustment of free networks. Here we fix one set of coordinate including x, y and z components in those pillar marks, and then obtain the coordinate differences with all other marks, i.e. the geocentric vectors $\Delta\mathbf{P}_{xyz}$ w.r.t. a fixed point in the network. These vectors can be transformed from the geocentric coordinate system to a topocentric coordinate system using surveyed geodetic longitude L and latitude B of the fixed point. It should be noted that this topocentric coordinate system can be named as a normal line topocentric system ENU_n, the transformation equation is as follows.

$$\mathbf{P}_{ENU_n} = \mathbb{R}_1\left(\frac{\pi}{2} - B\right)\mathbb{R}_3\left(\frac{\pi}{2} + L\right)\Delta\mathbf{P}_{xyz} \tag{1}$$

The detail definition of the rotation matrix $\mathbb{R}$ and the direction of rotation angle can be referred to App. A. On the other hand, in order to determine RP, the pillar marks also have their coordinates in LCN based on local leveling, trigonometric leveling and control surveying. Because there is a north orientation angle O_A between LCN and a topocentric coordinate system, which can be called as a vertical line topocentric system ENU_v. The transformation equation is as follows.

$$\mathbf{P}_{ENU_v} = \mathbb{R}_3\left(-O_A\right)\mathbf{P}_{loc} \tag{2}$$

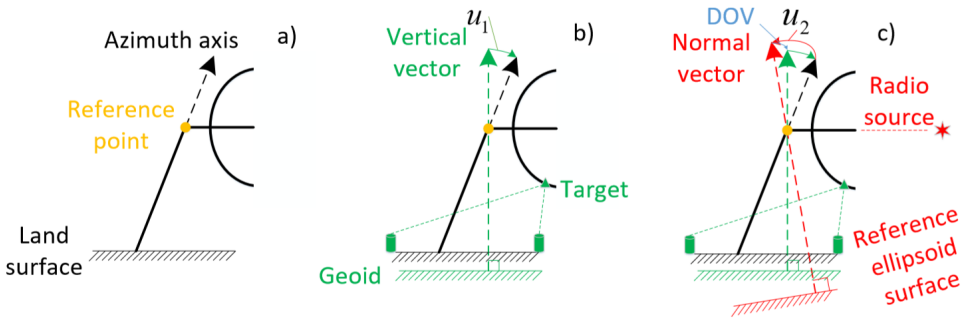

Figure 2. Schematic of DOV determination using axis information

where the value of O_A can be solved via the LCN orientation information or extracted from the estimates via an IM in RPD. Later we will solve the correction δA of O_A. Therefore, the selection of O_A aprior value will not affect the finally DOV estimates.

Here we got the two series of pillar mark coordinate in two different topocentric systems, i.e. ENU_v and ENU_n systems. With the identify fixed point as the origin of two systems, the rotation matrix $\mathbf{R}$ links the $\mathbf{P}_{ENU_n}$ and $\mathbf{P}_{ENU_v}$, which can be expressed in Eq. (3).

$$\mathbf{R} = \mathbf{R}_2(\eta)\,\mathbf{R}_1(\xi)\,\mathbf{R}_3(\delta A) = \begin{pmatrix} 1 & -\delta A & \eta \\ \delta A & 1 & -\xi \\ -\eta & \xi & 1 \end{pmatrix} \tag{3}$$

where the correction δA of O_A indicates the north orientation difference between two coordinate systems; all non-one elements in the right side of the equation in Eq. (3) are based on small angle approximation and high order neglect. These elements can be solved using Eq. (4) from the two groups of coordinates.

$$\begin{pmatrix} x_1 - x_0 \\ y_1 - y_0 \\ z_1 - z_0 \end{pmatrix} = \begin{pmatrix} 1 & 0 & 0 & 0 & z_0 & -y_0 \\ 0 & 1 & 0 & -z_0 & 0 & x_0 \\ 0 & 0 & 1 & y_0 & -x_0 & 0 \end{pmatrix} \begin{pmatrix} Tx & Ty & Tz & \xi & \eta & \delta A \end{pmatrix}^{\mathrm{T}} \tag{4}$$

where includes three translation parameters Tx, Ty and Tz, and three Euler angles ξ, η and δA. The positive directions of ξ and η are defined to the south and the east, respectively; the $\begin{pmatrix} x_0 & y_0 & z_0 \end{pmatrix}^{\mathrm{T}}$ and $\begin{pmatrix} x_1 & y_1 & z_1 \end{pmatrix}^{\mathrm{T}}$ represent the two groups of pillar mark coordinate difference series w.r.t. the fixed point in ENU_n and ENU_v, respectively. The parameter vector can be solve via the least square method. It may be noted that the scale factor can be also added into the parameter vector. However, since the size of LCN is small, there is a high ratio of the measuring error of GNSS baselines to their lengths, then the solved scale factor is in a magnitude of ppm (parts per million), rather than a real scale magnitude in ppb (parts per billion). Besides, the freedom of the error equation decreased as adding one more parameters. Therefore, we applied the 6-parameter SNCT rather than 7-parameter SNCT.

2.2 The Principle of AAII

The AAII use azimuth axis inclination angles solved by RPD and PC to determine the DOV of the radio telescope. As shown in Fig. 2, the relations among three vectors including antenna azimuth axis vector, local vertical(plumb) vector and local normal vector, are used to determine the DOV of VLBI station.

In Fig. 2 a, the azimuth axis of an alt-azimuth mount telescope is pointing to the local zenith approximately.

In Fig. 2 b, after the local RPD surveying is performed, i.e. the targets fastened on the telescope are observed using total stations or laser trackers with fixed level bubbles, the observed target trace points (TP) will form a set of scattered points with approximate spherical distribution. The reference point (RP) can be fitted by using these TP coordinates via different indirect methods (IM), refer to (Dawson et al., 2007; Lösler and Hennes, 2008; Lösler , 2009; Kallio and Poutanen, 2012; Li et al., 2013; Lösler et al., 2013; Ning et al., 2014). The RP position is the only goal that has always been concerned. In order to get a better post-fitted residual of TP coordinates or higher precision of RP position, in recent decades, some sophisticated IMs, e.g. Lösler (2008) modelled and fitted *axis related errors (ARE)* including an azimuth axis inclination angle u_1, which has two components and indicates that the azimuth axis is inconsistent with the local vertical vector.

In Fig. 2 c, the axis pointing errors can be modelled and calibrated via PC. Strong, point-like and well distributed radio source are scanned to obtain the differences between their observed and calculated directions. Later some PC models e.g. Guiar et al. (1987) and Zhao (2008) were introduced to fit AREs, and the AREs will be taken as parameters to substitute back into these models. This is the brief procedure of building PC models. In the AREs of the PC, there is also an azimuth axis inclination angle u_2, which indicates that the azimuth axis is inconsistent with the local normal vector.

Finally, the difference between u_1 and u_2 is the exact DOV of the telescope. The premise of the principle is that the LCN for RPD should be small enough so that the DOV values in the different parts of the LCN can be regarded the same and can be represented by the telescope.

Details of calculating azimuth inclination angles in the process of PC and RPD in this paper, can refer to App. B.1 and App. B.2, respectively.

3 Data, results and discussion

3.1 Data

3.1.1 RPD observations

In July and August 2011, PC and RPD tasks were performed at 25-m VLBI telescope in Nanshan, Urumqi. In order to determine the RP coordinate of the VLBI telescope, six pillars including a continuously GNSS operating reference station (code: GUAO) are built around the telescope and form a LCN, see the black triangles and blue segments in Fig. 3. The green arrow from P2 to P1 represents the x direction or the orientation of the LCN. The precisions of pillars determined via GNSS and local triangle measuring are shown in Tab. 1 and Tab. 2, respectively. The coordinates of the pillars were solved by using more than 1 week GNSS synchronous loop observing. The detailed GNSS and RPD observing, and local TP data reduction can be found in papers (Zhang et al. (2013a) and Zhang et al. (2015)). Total 233 scatted TPs were observed to determine its RP and AREs. The three pillars of highest precision are P1, P2 and P4. The P3 is lower and P5 is the worst in precision.

3.1.2 PC observing

As an irregularly scheduled but necessary task, the period of telescope PC is about several months. The Urumqi station applies a 22-parameters PC fitting model, in which the ARE definition is identified to those in our model, as shown in Eq. (B.8). The corrected pointing accuracy is ∼7" by using the PC fitting model. Because there is a telescope rebuilding in 2014, it is impossible to playback the situation of the 25-m telescope in 2011 again. Therefore, it has to assume that each item in the right hand side in Eq. (B.8)

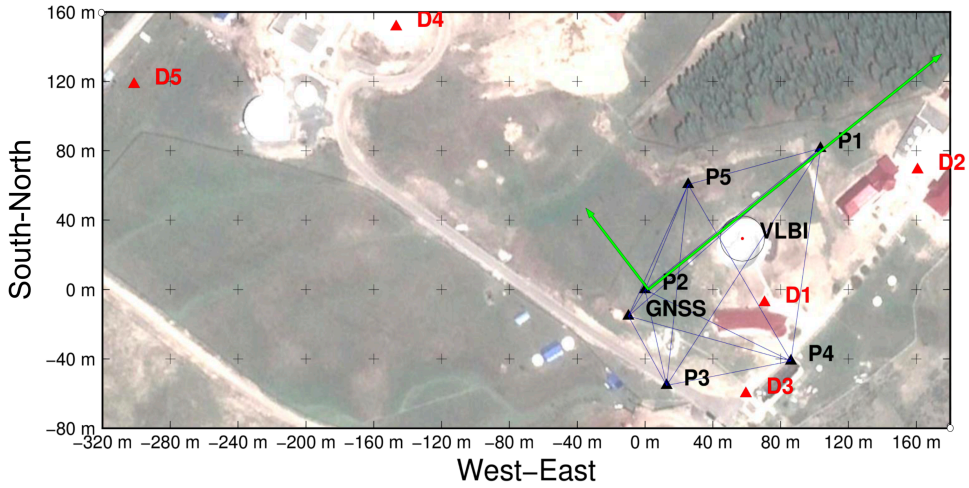

Figure 3. Pillars in LCN (black triangles) and Observing DOV points(red triangles) in Urumqi station

Table 1. GNSS geocentric coordinates and their precisions of five pillar marks in LCN (unit in meters)

Pillar	X	Y	Z	m_X	m_Y	m_Z
P1	228261.9520	4631878.2174	4367091.1883	0.0004	0.0004	0.0004
P2	228368.3572	4631933.8043	4367036.7234	0.0004	0.0004	0.0004
P3	228357.4957	4631972.0838	4366996.2451	0.0004	0.0004	0.0004
P4	228283.8955	4631969.0645	4367009.3896	0.0004	0.0004	0.0004
P5	228340.6229	4631889.2121	4367076.7383	0.0005	0.0005	0.0005

has the same contribution to the telescope pointing, then the sigma of the azimuth inclination angle α or β is 3∼4".

3.1.3 DOV measurements

In May 2020, according to the different accuracies requirements of the the military specification for astronomic surveys (GJB 149-2013), the DOVs of different points in Urumqi station were surveyed using AT330-type digital zenith camera positioning system (also known as zenith tube, as shown in Fig. 4). Considering the limitations of observing periods caused by the weather and the range of hardening ground in the station, as shown in Fig. 3 and Table 3, the zenith tube calibration and its operation mode are flexibly configured, e.g. at D1, "1+4" model was performed, in which "1" indicates measuring once inclinometer parameters first and then taking sky pictures in zenith and simultaneously measuring inclinometer parameters for "4" times via changing the symmetrical positions of the zenith tube on the supporting platform step by step. Due to the bad weather, only "1+1" was performed at D3. However, the D2, D4 and D5 are of "1+3" model.

Although there may be a secular variation in DOV value from 2011 to 2020, as the result of surveyed DOVs in Beijing and Yunnan region, it shows their variations are within 0.001 ∼ 0.004"/yr and they vary from place to place. If the DOV in Urumqi station has similar changes, then the DOV difference after 9 yr will be no more than 0.04".

Figure 4. The used AT330-type zenith tube at D4 point waiting for a sunset.

Table 2. Coordinates and their precisions in LCN via local triangle measuring (unit in meters)

Pillar	x	y	z	m_x	m_y	m_z
P1	131.6649	0.0000	−6.6053	0.0008	0.0000	0.0002
P2	0.0000	0.0000	0.0000	0.0000	0.0000	0.0000
P3	−24.1466	−51.3691	−0.5064	0.0018	0.0011	0.0002
P4	42.2576	−85.5874	3.7326	0.0004	0.0005	0.0002
P5	57.5048	31.9157	−5.7958	0.0005	0.0003	0.0002

Table 3. The real surveyed DOV value of 5 points

Point	Longitude:dms	Latitude:dms	ξ :”	η :”
D1	87 10 41.971	43 28 16.455	32.776 ± 0.0477	11.382 ± 0.0466
D2	87 10 45.984	43 28 18.935	32.787 ± 0.0244	11.333 ± 0.0248
D3	87 10 41.477	43 28 14.785	32.563 ± 0.0557	11.376 ± 0.1642
D4	87 10 32.309	43 28 21.613	33.262 ± 0.0471	10.918 ± 0.0607
D5	87 10 25.432	43 28 20.544	33.602 ± 0.0672	10.864 ± 0.0488

Table 4. Some AREs solved by PC and RPD models

	Parameter	PC model	RPD model
1	α / α' (")	9.0±4.0	−2.9±3.3
2	β / β' (")	−43.0±4.0	−27.7±3.2
3	γ (")	−22.1±4.0	−24.8±5.9
4	e (mm)	0.7±0.0	−0.8±0.4

Table 5. DOV results calculated by different models, unit:"

	Models	$\eta_\odot$	$\xi_\odot$
1	AAII	11.9 ± 5.0	−15.3 ± 5.0
2	SNCT	11.1 ± 4.7	−30.5 ± 4.4
3	EGL	10.8 ± 4.1	−30.6 ± 11.6
4	MIM	15.8	−42.5
5	CGGM2000	11.8 ± 1.5	−32.8 ± 1.5
6	Real surveying	11.4 ± 0.0	−32.7 ± 0.0

3.2 Results

3.2.1 ARE consistence

Some estimated AREs in PC fitting model and IM are listed in Tab. 4, where the e estimated from PC model is 151.76" and it can transform to 0.7 mm by taking the meter as a unit. There is a good agreement in γ, while the difference of e is 1∼2 mm.

3.2.2 DOV consistence

Two different definitions of DOV components η and ξ are applied in this paper. By defaults, $\eta_\odot$ and $\xi_\odot$ indicate zenith DOV components, the definitions of $\eta_\odot$ and $\xi_\odot$ are to the east and to the south, respectively. In some paragraphs, $\eta_\otimes$ and $\xi_\otimes$ are DOV components pointing to the ground, i.e. to the west and to the north, respectively.

The value of $\eta_\odot$ and $\xi_\odot$ in Urumqi VLBI station solved by the relations of azimuth inclination angles are 11.9" and −15.3", respectively. The preliminarily evaluated formal error is ∼ 5" for $\eta_\odot$ or $\xi_\odot$.

Beside of using SNCT, AAII and real surveyed DOV as mentioned above, *mass integration model(MIM)* and CGGM2000 are also applied to check the results and to test the accuracy of different models. The details of MIM are introduced in App. C. The CGGM2000 is a DOV model of 1" x 1" resolution. The mean accuracy of any point in the main land of China tested by CGGM2000 can reach up to ±1.5", as shown in Sun et al. 2005, which used 1489 high precision astro-geoid points.

The corresponding DOV results based on different methods are shown in Tab. 5.

3.3 Discussion

In Tab. 5, it shows a large absolute DOV value in Urumqi, especially in the north direction (−32.7"), since the main peaks of Tianshan mountain locate in the south of the Urumqi station.

The real surveying DOV in Tab. 5 refers DOV value measured at D1 since it is the closest point to the VLBI telescope. We take it as a reference, i.e. the most reliable result, to analysis the DOVs solved by other methods. On the whole, except for a large absolute value of DOV in MIM, which is due to the simplification of no isostasy, and a small absolute value of DOV in the north direction of AAI, all other DOV components agree well.

The DOVs solved via SNCT and EGL are determined by using 3 identified higher precision pillar marks including P1, P2 and P4. The result shows the high accuracy DOV can be obtained by 3 pillar marks of the widest coverage area and the highest coordinate accuracy. Besides, some points of lower accuracy may contaminate the certainty of DOV value if SNCT and EGL are applied. The detail of the DOV error propagation in EGL and the accuracy analysis in SNCT can refer to Ma et al. (2021). In SNCT, the estimated DOV is related to the precision and the number of point, geometry and area of the network. There is a same formal error in west-east direction for SNCT and EGL, while in south-north direction, the formal error in DOV of SNCT is less than that in EGL. Besides, the derivation and error adjustment of SNCT is simpler than that of EGL and are suitable for promotion. Besides, compared to optical DOV observing, the SNCT method has some advantages including measuring in all-weather and all-time.

The difference between MIM and the real surveying value is 4.4" in $\eta_{\odot}$ while it is −9.8" in $\xi_{\odot}$, which indicates the difference of isostasy in different directions. The DOV solved by CGGM2000 has a good agreement with the real value.

The DOV solved by AAII shows a difference of −17.4" in $\xi_{\odot}$. It is caused by the north-south asymmetric or non-uniformly distributed sky coverage of the selected radio calibration sources above the local zenith of the station. The Urumqi telescope was rebuilt in 2014. Hence the state of the telescope in 2011 can be not retroactive. To explain the problem, here we show a typical radio calibration source sky coverage for PC of Tianma VGOS telescope in Shanghai, as shown in Fig. 5 . Total 5 sources were observed and their traces (sky coverage) are nearly symmetric in the west and east, while it is extremely asymmetric in the north south direction. However, the normal equation will not be singularity while estimating ARE parameters. The parameter α and β appear in both Eq. (B.5) and (B.5). They have a magnitude differences of $\frac{1}{2}\lambda\beta$ and $\frac{1}{2}\lambda\alpha$, respectively. The differences are caused by the high order terms of AREs and their magnitudes will be no greater than 0.01". Hence, we can check the consistencies of the α and the β estimated by the two equations. The results show that the consistencies of the α and β are −3.0 ± 2.1" and 5.9 ± 2.3", respectively. It indicate that the north-south asymmetric of radio source sky coverage is the reason of difference. In Urumqi, the 22 item PC model were introduced to fit AREs in PC, the coefficients in front of item $cosAsinE$ and $sinAsinE$ in azimuth pointing calibration equation are extracted as $-\alpha$ and β, respectively.

On the other hand, the azimuth axis inclination angle modelled from RPD, i.e. α' and β' are estimated using the Lösler's IM, see App. B.2, then the DOV is calculated by AAII based on a unified PC and RPD model, see App. B.

3.4 Precision evaluation

In the case of Urumqi, the DOV representativeness can be inferred from its real surveyed values. As shown in Tab. 5 and Fig. 3, within the range of 200 m and 500 m, the DOV consistencies are ∼0.4" and ∼1", respectively. It indicates that the longest base-

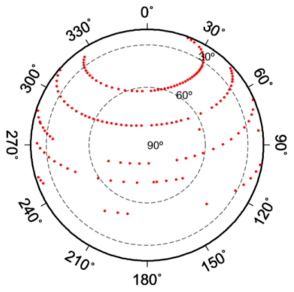

Figure 5. The calibrating radio source sky coverage above Tianma VGOS station in an experiment.

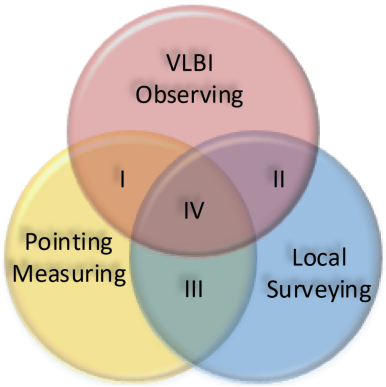

Figure 6. Relations among VLBI obseving, local surveying and pointing measuring

line in the LCN should be within 500 m, if the precision requirement of the DOV is less than 1". Considering the principle of SNCT, if the longest baseline of LCN is 500 m and the DOV precision requirement is less than 1", then the requirement of the pillar precision of GNSS position should be less than $500/1/206265 \approx 0.002$ m, which is achievable under the current GNSS measuring accuracy. On the other hand, if we have the mean precision of GNSS pillars of 0.4 mm and the longest baseline in LCN is shorter than 200 m, then the DOV precision of 0.4" can be expected. In the same manner, if the DOV variation in a small range satisfies a linear condition, in order to obtain a DOV precision of 0.1", the longest baseline in LCN probability be less than 50 m and the GNSS pillar precision should be better than 2 mm. However, this kind of LCN may be only suitable for very small antennas.

In our case, the mean precision of the 3 pillars is ∼1 mm, which is the total uncertainty including uncertainties in LCN and in geocentric systems, and the longest baseline in LCN is ∼160 m, then the theoretical precision of DOV should be ∼1". The result also reflects that the current precisions of local surveying and GNSS observing are the bottleneck of DOV determination in VLBI station. Hence, the improvement of their observing precision and accuracy will be prerequisites for realizing high-precision DOV monitoring.

4 Conclusions

By unifying the models of telescope structure in IM and PC, we can expect to deduce or monitor a VLBI station DOV with zero cost and the precision of 1 arcsecond

or better, providing that RPD and PC are necessary tasks to maintenance the telescope, especially for a new-built telescope.

Owing to introducing a local levelling from RPD, VLBI telescope will be no more insensitive to the gravity. Thereby VLBI could be closer to realise all three goals in geodesy, i.e. geometry, rotation measuring and sensing the direction of gravity.

As shown in Fig. 6, in geodetic VLBI, our methods link the three tasks including VLBI delay observing, PC surveying and RPD measuring. Their relations are list as follows:

I: VLBI observing is under the premise of good PC surveying. The PC surveying offers a pointing correction model to the VLBI antenna.

II: The RP coordinate of VLBI telescope can be solved via VLBI delay or local RPD based on GNSS. The agreement of RPs determined by the different techniques has important sense to constrain multi-tech TRF and to discern systematic errors.

III : As known in the above, PC and RPD can be connected by the DOV, then each one among them can be solved, e.g. if we have only DOV and AREs solved from RPD, then a preliminary model for PC can be obtained. It will greatly reduce the time required for iterative PC determination.

IV : The AO links three tasks, which is also an important indicator to discern multi-tech systematic errors. The discrepancy of AO solved by different agencies could reach up to 4 mm, while the discrepancy of AO solved from VLBI delay and local RPD has the same magnitude of 4∼5 mm (Krásná et al. , 2014; Nilsson , 2015; Kurdubov , 2010). For a long time, the physical meaning of estimates in PC modelling has been neglect to research. Now the AO, the coefficient in front of the item $sinE$ in elevation PC model, should be included in conventional systematic error monitoring. In addtion, we also recommend that axis inclination should be included in VLBI telescope modelling.

Traditionally, in PC, accuracy and relevance of the ARE parameters have been not concerned. This conclusion is also suitable for the case of PC observing in Urumqi in 2011. In the future PC work, we will pay much attention to improve the source sky coverage and correlation among ARE parameters, then a high precision azimuth axis inclination angle could be obtained to calculate a high precision DOV.

A Definitions

Although both PC and RPD modelled the structure of telescope, due to their different functions, they are mutually independent all the time as mentioned above. Thus, it is foremost to unify the axis related parameter definitions in two models. Besides, this section will also give definitions on different coordinate systems and different angle directions.

To unify PC and RPD models, we directly derive the complete ARE expression in PC model, in which some ARE definitions are in accordance with those in the Lösler's IM.

A.1 Coordinate systems

Three coordinate systems are applied including topocentric coordinate system OENU, telescope-fixed coordinate system Oxyz and a tangent plane coordinates system in pointing direction, which all belong to Cartesian coordinate system (right-hand coordinate system), as shown in Fig. 2.

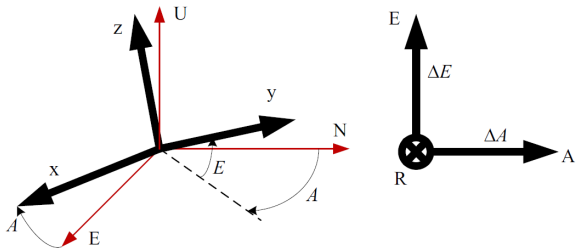

Figure A.1. Schematic of three coordinate systems

Reference point O is taken as their common origins, which is defined as the intersection point between the azimuth-axis and elevation-axis of the telescope. If these axes do not intersect, the reference point is the projection of the elevation- axis onto the azimuth-axis which has the shortest/ minimum distance to the elevation-axis (Lösler and Hennes, 2008).

The direction of three axes in the topocentric coordinate system OENU are the East, the North and the zenith, respectively.

In the telescope-fixed coordinate system $Oxyz$, x is the telescope elevation axis, and the second axis y is the telescope pointing direction. The third axis z is perpendicular to the plane contains the O and xy axes.

In the tangent plane coordinates system OARE, the second axis R is consistent with the telescope pointing direction. The A and E are in the tangential directions of azimuth and elevation, respectively.

Two kinds of rotation matrix are introduced in this paper. One is used to describe the new point position after a rotation in the same coordinate system, represented by $\mathbf{R}_{1/2/3}$, where 1/2/3 indicate the rotation w.r.t. the first, second and third rotation axis, respectively, the other is applied to describe the transformation of point position in new coordinate system w.r.t. old coordinate system, represented by $\mathbb{R}_{1/2/3}$ and the subscript means as the same as above.

A.2 Positive and negative angles

Angles are the inputs for the different rotation matrix. In Cartesian coordinate system, the positive direction of rotation angle is defined as follows : fix x and rotate from y to z; fix y and rotate from z to x; fix z and rotate from x to y. Conversely, the rotation angle should be negative.

The positive angles mentioned in this paper are α、β 、γ、δ、μ and E. The negative angles include λ and A. Herein, E and A are azimuth and elevation angles, respectively. Other meanings of symbol can refer to App. A.3 in detail.

A.3 Axis related errors

The AREs modelled in the paper are listed in Tab. A.1, where we use δ for representing a horizontal collimation error in space, which varies its effect ΔA on the azimuth with the elevation angle changing, as shown in Fig. A.2, since telescope collimation error reflects a 2-dimensional difference between real and designed pointing direction in space. The vertical collimation error is absorbed in elevation zero position error. In Tab. A.1, first six items belong to axis inclination measured by angle, while the last

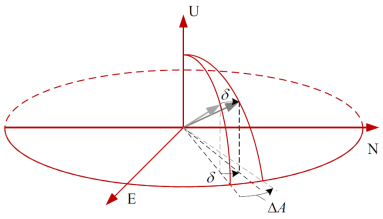

Figure A.2. Effect on azimuth pointing error cause by horizontal collimation error.

Table A.1. The AREs and their corresponding symbols

Numb.	Name	Symbol
1	Azimuth axis inclination angle (to the east)	α
2	Azimuth axis inclination angle (to the south)	β
3	Horizontal collimation error	δ
4	Elevation axis inclination angle	γ
5	Azimuth encoder fixed offset	λ
6	Elevation encoder fixed offset	μ
7	Axis offest (AO)	e

item e is the offset between azimuth and elevation axes measured by distance. The positive direction for e points along with the horizontal direction of telescope.

B Unified PC and RPD model derivation

B.1 PC model deduction

The PC model is based on scanning radio sources. Therefore, it provides a normal line through the RP of the telescope. The steps for ARE effect on telescope pointing are as follows.

1. Initially, two systems $Oxyz$ and $OENU$ overlap each other. At this moment, both telescope azimuth and elevation angles are zero. Suppose that a point p is in the pointing direction of the telescope and has a distance from RP of 1. Here is a vector of $\mathbf{P} = (\ 0 \quad 1 \quad 0\ )^{\mathrm{T}}$.

2. The horizontal collimation error δ, elevation variation $E+\mu$, AO e, elevation axis inclination angle γ, azimuth variation $A+\lambda$, azimuth inclination angles α and β are introduced successively, as shown in Fig. B.1. Thus the new position $\mathbf{P}'$ of point p in OEUN will be

$$\mathbf{P}' = \mathbf{R}_1(\beta)\mathbf{R}_2(\alpha)\mathbf{R}_3(-A-\lambda)\mathbf{R}_2(\gamma)\left[\mathbf{e}+\mathbf{R}_1(E+\mu)\mathbf{R}_3(\delta)\mathbf{P}\right] \tag{B.1}$$

where $\mathbf{e}$ is an AO vector.

3. If the real (observed) position of the observed radio source determined by scanning its maximum flux in space are A_o and E_o, then a new expression $\mathbf{P}''$ of p in OARE can be transformed by Eq. (B.2).

$$\mathbf{P}'' = \mathbb{R}_1(E_o)\mathbb{R}_3(-A_o)\mathbf{P}' \tag{B.2}$$

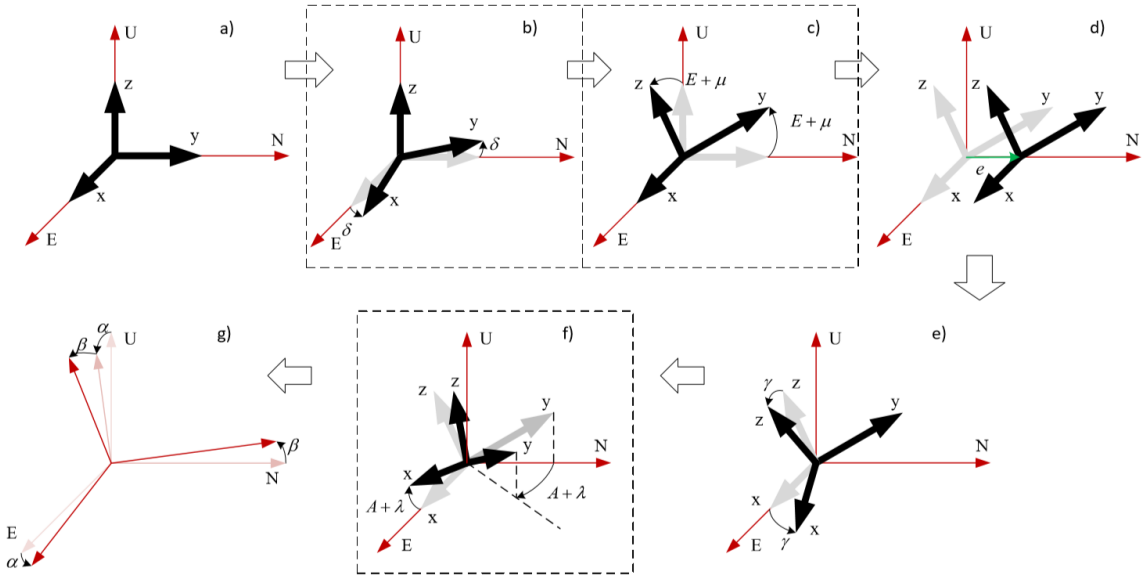

Figure B.1. Deduction for ARE effect on telescope pointing.

The point p is fixed on the pointing direction of the telescope as mentioned above, then its calculated position can be also represented by $\mathbf{P}$ in OARE. Hence the telescope ARE PC model $\mathbf{C}$ will be given in Eq. (B.3).

$$\mathbf{C} = \mathbf{P}'' - \mathbf{P} = \begin{pmatrix} \Delta_A & \Delta_R & \Delta_E \end{pmatrix}^{\mathrm{T}} \tag{B.3}$$

Let $A_o = A; E_o = E$, and simplify the sine and cosine forms of small angles, e.g. $\cos\alpha = 1$; $\sin\alpha = \alpha$. It yields that

$$\begin{cases} \mathbf{C} = \begin{pmatrix} \mathbf{A}(\mathbf{C_A} \bullet \mathbf{C_c})\mathbf{A^T} & \mathbf{A}(\mathbf{C_R} \bullet \mathbf{C_c})\mathbf{A^T} & \mathbf{A}(\mathbf{C_E} \bullet \mathbf{C_c})\mathbf{A^T} \end{pmatrix}^{\mathbf{T}} \\ \mathbf{C_c} = \mathbf{V_E^T V_A} \\ \mathbf{V_A} = \begin{pmatrix} 1 & \cos A & \sin A & \cos 2A & \sin 2A \end{pmatrix} \\ \mathbf{V_E} = \begin{pmatrix} 1 & \cos E & \sin E & \cos 2E & \sin 2E \end{pmatrix} \end{cases} \tag{B.4}$$

where $\mathbf{A} = \begin{pmatrix} 1 & 1 & 1 & 1 & 1 \end{pmatrix}$; The form of $\mathbf{A}(\mathbf{M})\mathbf{A^T}$ in Eq. (B.4) is applied to calculate the sum of all the elements in $\mathbf{M}_{5\times5}$; The symbol "•"represents a dot product; $\mathbf{C_c}$ is a harmonic term matrix; The three elements in $\mathbf{C}$, from left to right, are the pointing bias in azimuth, radial and elevation, respectively. Their positive directions are consistent with the defined coordinate in Fig. A.1 right. The PC model of the telescope is the form of adding a negative sign to all elements in the $\mathbf{C}$. Detail constitution of $\mathbf{C_A}$, $\mathbf{C_R}$ and $\mathbf{C_E}$ are listed in coefficient matrix, as shown in Eqs. (B.5), (B.6) and (B.7), respectively.

$$\mathbf{C_A} = \begin{pmatrix} -\delta + e\lambda - \frac{1}{2}e\alpha\beta - \frac{1}{2}\lambda\alpha\beta\delta & \alpha\delta\gamma & \beta\delta\gamma & \frac{1}{2}e\alpha\beta + \frac{1}{2}\lambda\alpha\beta\delta & \frac{1}{2}\alpha\beta\delta - \frac{1}{2}e\lambda\alpha\beta \\ \lambda + \mu\gamma - \frac{1}{2}\alpha\beta + \frac{1}{2}\lambda\mu\alpha\beta\gamma & \mu\alpha & \mu\beta & \frac{1}{2}\alpha\beta - \frac{1}{2}\lambda\mu\alpha\beta\gamma & -\frac{1}{2}\lambda\alpha\beta - \frac{1}{2}\mu\alpha\beta\gamma \\ \gamma - \lambda\mu + \frac{1}{2}\mu\alpha\beta + \frac{1}{2}\lambda\alpha\beta\gamma & \alpha & \beta & -\frac{1}{2}\mu\alpha\beta - \frac{1}{2}\lambda\alpha\beta\gamma & -\frac{1}{2}\alpha\beta\gamma + \frac{1}{2}\lambda\mu\alpha\beta \\ 0 & 0 & 0 & 0 & 0 \\ 0 & 0 & 0 & 0 & 0 \end{pmatrix} \tag{B.5}$$

$$\begin{cases} \mathbf{C_R} = \begin{pmatrix} \mathbf{C_{R,5\times3}} & \mathbf{C_{R,5\times2}} \end{pmatrix} \\ \mathbf{C_{R,5\times3}} = \begin{pmatrix} -\frac{1}{2}\lambda\mu\gamma + \frac{1}{4}\lambda\alpha\beta + \frac{1}{4}\mu\alpha\beta\gamma & -\mu\beta - \frac{1}{2}\alpha\gamma + \frac{1}{2}\lambda\mu\alpha - \frac{1}{2}\lambda\beta\gamma & \mu\alpha - \frac{1}{2}\beta\gamma + \frac{1}{2}\lambda\mu\beta + \frac{1}{2}\lambda\alpha\gamma \\ e + \lambda\delta - \frac{1}{2}\alpha\beta\delta + \frac{1}{2}e\lambda\alpha\beta & -\beta\delta\gamma & \alpha\delta\gamma \\ \delta\gamma & e\beta + \alpha\delta - e\lambda\alpha + \lambda\beta\delta & -e\alpha + \beta\delta - e\lambda\beta - \lambda\alpha\delta \\ -\frac{1}{2}\lambda\mu\gamma + \frac{1}{4}\lambda\alpha\beta + \frac{1}{4}\mu\alpha\beta\gamma & \frac{1}{2}\alpha\gamma - \frac{1}{2}\lambda\mu\alpha + \frac{1}{2}\lambda\beta\gamma & \frac{1}{2}\beta\gamma - \frac{1}{2}\lambda\mu\beta - \frac{1}{2}\lambda\alpha\gamma \\ -\frac{1}{2}\lambda\gamma + \frac{1}{4}\alpha\beta\gamma - \frac{1}{4}\lambda\mu\alpha\beta & -\frac{1}{2}\lambda\alpha - \frac{1}{2}\mu\alpha\gamma - \frac{1}{2}\lambda\mu\beta\gamma & -\frac{1}{2}\lambda\beta - \frac{1}{2}\mu\beta\gamma + \frac{1}{2}\lambda\mu\alpha\gamma \end{pmatrix} \\ \mathbf{C_{R,5\times2}} = \begin{pmatrix} \frac{1}{4}\lambda\alpha\beta + \frac{1}{4}\mu\alpha\beta\gamma & \frac{1}{4}\alpha\beta - \frac{1}{4}\lambda\mu\alpha\beta\gamma \\ -\frac{1}{2}\alpha\beta\delta + \frac{1}{2}e\lambda\alpha\beta & \frac{1}{2}\lambda\alpha\beta\delta + \frac{1}{2}e\alpha\beta \\ 0 & 0 \\ \frac{1}{4}\lambda\alpha\beta + \frac{1}{4}\mu\alpha\beta\gamma & \frac{1}{4}\alpha\beta - \frac{1}{4}\lambda\mu\alpha\beta\gamma \\ \frac{1}{4}\alpha\beta\gamma - \frac{1}{4}\lambda\mu\alpha\beta & -\frac{1}{4}\mu\alpha\beta - \frac{1}{4}\lambda\alpha\beta\gamma \end{pmatrix} \end{cases} \tag{B.6}$$

$$\begin{cases} \mathbf{C_E} = \begin{pmatrix} \mathbf{C_{E,5\times3}} & \mathbf{C_{E,5\times2}} \end{pmatrix} \\ \mathbf{C_{E,5\times3}} = \begin{pmatrix} \mu + \frac{1}{2}\lambda\gamma - \frac{1}{4}\alpha\beta\gamma + \frac{1}{4}\lambda\mu\alpha\beta & \beta - \frac{1}{2}\lambda\alpha - \frac{1}{2}\mu\alpha\gamma - \frac{1}{2}\lambda\mu\beta\gamma & -\alpha - \frac{1}{2}\lambda\beta - \frac{1}{2}\mu\beta\gamma + \frac{1}{2}\lambda\mu\alpha\gamma \\ \delta\gamma & e\beta + \alpha\delta - e\lambda\alpha + \lambda\beta\delta & -e\alpha + \beta\delta - e\lambda\beta - \lambda\alpha\delta \\ -e - \lambda\delta + \frac{1}{2}\alpha\beta\delta - \frac{1}{2}e\lambda\alpha\beta & \beta\delta\gamma & -\alpha\delta\gamma \\ -\frac{1}{2}\lambda\gamma + \frac{1}{4}\alpha\beta\gamma - \frac{1}{4}\lambda\mu\alpha\beta & -\frac{1}{2}\lambda\alpha - \frac{1}{2}\mu\alpha\gamma - \frac{1}{2}\lambda\mu\beta\gamma & -\frac{1}{2}\lambda\beta - \frac{1}{2}\mu\beta\gamma + \frac{1}{2}\lambda\mu\alpha\gamma \\ \frac{1}{2}\lambda\mu\gamma - \frac{1}{4}\lambda\alpha\beta - \frac{1}{4}\mu\alpha\beta\gamma & -\frac{1}{2}\alpha\gamma + \frac{1}{2}\lambda\mu\alpha - \frac{1}{2}\lambda\beta\gamma & -\frac{1}{2}\beta\gamma + \frac{1}{2}\lambda\mu\beta + \frac{1}{2}\lambda\alpha\gamma \end{pmatrix} \\ \mathbf{C_{E,5\times2}} = \begin{pmatrix} -\frac{1}{4}\alpha\beta\gamma + \frac{1}{4}\lambda\mu\alpha\beta & \frac{1}{4}\mu\alpha\beta + \frac{1}{4}\lambda\alpha\beta\gamma \\ 0 & 0 \\ \frac{1}{2}\alpha\beta\delta - \frac{1}{2}e\lambda\alpha\beta & -\frac{1}{2}e\alpha\beta - \frac{1}{2}\lambda\alpha\beta\delta \\ \frac{1}{4}\alpha\beta\gamma - \frac{1}{4}\lambda\mu\alpha\beta & -\frac{1}{4}\mu\alpha\beta - \frac{1}{4}\lambda\alpha\beta\gamma \\ -\frac{1}{4}\lambda\alpha\beta - \frac{1}{4}\mu\alpha\beta\gamma & -\frac{1}{4}\alpha\beta + \frac{1}{4}\lambda\mu\alpha\beta\gamma \end{pmatrix} \end{cases} \tag{B.7}$$

The Eqs. (B.4)-(B.7) are the generalized expression of the ARE effect in telescope pointing. In order to ensure the accuracy of ARE pointing model less than several as, quadratic and higher-order terms, e.g. $\frac{1}{2}\lambda\gamma$ and $\frac{1}{4}\alpha\beta\gamma$, can be dropped. Then a simplified ARE pointing bias and a PC model are obtained as Eq. (B.8) and Eq. (B.9), respectively.

$$\begin{cases} \Delta_A = -\delta + \lambda\cos E + \gamma\sin E + \alpha\cos A\sin E + \beta\sin A\sin E \\ \Delta_E = \mu - e\sin E + \beta\cos A - \alpha\sin A \end{cases} \tag{B.8}$$

$$\begin{cases} \sigma_A = -\Delta_A \\ \sigma_E = -\Delta_E \end{cases} \tag{B.9}$$

The Eq. (B.8) is similar to the commonly used ARE PC model in Guiar et al.. Actually, the model in Guiar et al. is deducted ARE dispersedly and then combines the effect on the pointing together, which is an indirect combination model without high-order terms. In Eq. (B.8), it is clear that azimuth inclination angles (α and β) impacts on both azimuth and elevation pointing accuracies.

B.2 Indirect Method

Generally, the IM is applied to determine the RP of telescope. Lösler (2009) proposed an IM could also fit some ARE of the telescope. It builds the relation among AREs including α', β', γ, e and the calculated position $\mathbf{P}_{calc}$ of TP, which is given as follows

$$\begin{aligned} \mathbf{P}_{calc} = \mathbf{P}_{rp} + \mathbf{R}_1(\beta')\cdot\mathbf{R}_2(\alpha')\cdot\mathbf{R}_3(A+O_A) \\ \cdot\mathbf{R}_2(\gamma)\cdot\mathbf{R}_1(E+O_E)\cdot(\mathbf{P}_{tel}+\mathbf{e}), \end{aligned} \tag{B.10}$$

where O_A and O_E are initial azimuth angle and elevation angle, respectively. The O_A not only includes the λ in Sect. A.3 and Fig. B.1 f, but also contains the orientation difference between the north and the orientation axis in local control surveying network; The O_E includes the μ and the angle between target pointing direction and telescope pointing direction, see in Fig. B.1 c; The δ mentioned in Sect. A.3 and Fig. B.1 b are absorbed by TP position vector $\mathbf{P}_{tel}$; The definitions of A,E,γ and $\mathbf{e}$ are identical to those in Sect. A.3. Since the RP determination is based on the local height datum, the up in OENU means the oppsite direction of the local plumb line over the RP, i.e. the α' and β' represent the inclination angles of azimuth axis w.r.t. the local vertical.

The RP position and AREs in Eq. (B.10) can be estimated by building and solving error equations (Koch, 2014). During the estimation, reweighting method (Gipson, 1997) is applied to adjusting the weight of TPs in order to getting a unity of χ^2/f, where f is the degree of freedom in error equation.

B.3 DOV calculation

As mentioned in App. B.1 and App. B.2, the α and β are the azimuth axis inclination angles of deviation from the local normal vector, while α' and β' obtained by IM are the azimuth axis inclination angles of deviation from the local vertical vector. For the same antenna in the same period, the pointing of the azimuth axis are fixed in space, then it implies that the DOV of the VLBI station can be calculated by Eq. (B.11).

$$\begin{cases} \eta_{\odot} = \alpha - \alpha' \\ \xi_{\odot} = \beta - \beta' \end{cases} \tag{B.11}$$

where DOV can have two reverse directions, pointing to the underground or to the zenith, w.r.t. local normal vector, which has a sign difference. The DOV angles $\eta_{\odot}$ and $\xi_{\odot}$ are the zenith inclination components to the east and to the south, respectively.

C MIM

In the matter integration model, no isostasy is considered. A digital elevation model around the Urumqi station is introduced to calculate the differences of the distribution of surface mass in east and in north are calculated respectively. The equation for calculating the gravity anomaly in each direction is given in Eq. (C.1).

$$\Delta g = G \int_0^R \int_{\theta_0}^{\theta_1} \int_{H_B - H_0}^{H_U - H_0} \frac{\rho r}{r^2} dr d\theta dh \tag{C.1}$$

where, G is the gravitational constant; R is horizontal integration radius and the upper bound of 30 km is chosen in our case, since the integration area will reach up to the main peaks of Tianshan Mountain if we select a longer radius, as shown in Fig. C.1; θ_1 and θ_0 are the upper and lower bounds of the angle in circle integral, respectively; H_U and H_B are the upper and lower bounds of the elevation after a round table was filled, respectively; ρ is the density of rock. We use two symmetrical half round table to calculate each component of Δg_{WE} or Δg_{NS}, which indicates the west-east or the north-south gravity anomaly, respectively. Besides, the extra gravity anomaly Δg_o induced by overlapped mass is also excluded from Δg_{WE} and Δg_{NS}, then the DOV $\eta_{\otimes,m}$ and $\xi_{\otimes,m}$ calculated by the mass integration model will given by Eq. (C.2), where ϕ and H_0 are the latitude and the height of the Urumqi station, respectively. The applied integration bounds are listed in Tab. 4.

$$\begin{cases} \eta_{\otimes,m} = 206265 \cdot \frac{\Delta g_{WE} - \frac{\sqrt{2}}{2}\Delta g_o}{g} \\ \xi_{\otimes,m} = -206265 \cdot \frac{\Delta g_{SN} - \frac{\sqrt{2}}{2}\Delta g_o}{g} \\ g = 980.612 - 2.5865\cos 2\phi + 0.0058\cos^2 2\phi - 0.000308 H_0 \end{cases} \tag{C.2}$$

Acknowledgments

We acknowledge Dr. Anmin Zeng and Dr. Shouzhou Gu for their help for the DOV calculation using the CGGM2000 model. The first author is grateful for the valuable suggestions from Dr. Jin Li and Prof. Chengli Huang. The team members from the 1001st factory, Nanshan station and 61243 troops are thanked for the hard field work. Several

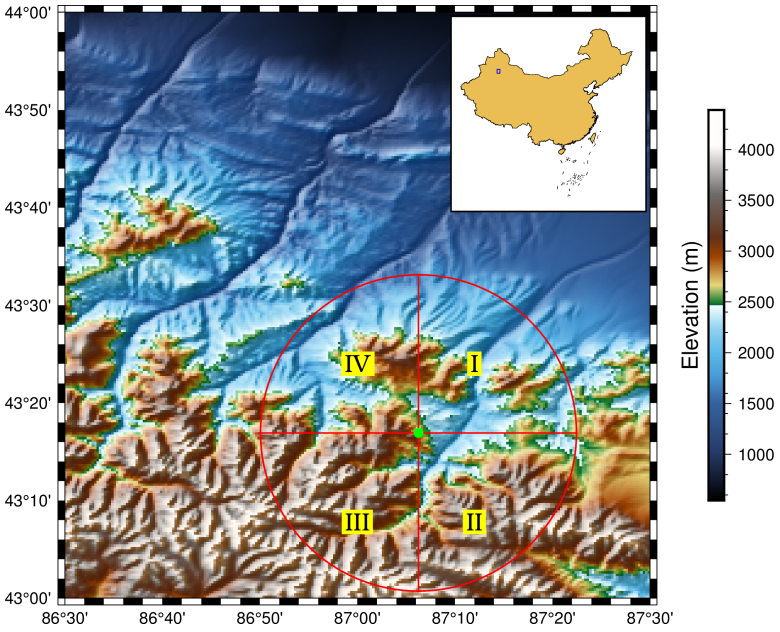

Figure C.1. The location of Urumqi station in China and the integration range of the MIM.

Table C.1. The applied upper and lower bounds to calculate Δg

	Δg_{WE}	Δg_{NS}	Δg_o
θ_0	$\frac{\pi}{2}$	π	π
θ_1	$\frac{3\pi}{2}$	2π	$\frac{3\pi}{2}$
H_B^{30km}	1902.12	1675.58	1902.12
H_U^{30km}	2238.91	2496.47	2238.91

plots were made with the General Mapping Tool (GMT) software (Wessel and Smith 1998), available at http://gmt.soest.hawaii.edu under the GNU General Public License. Some icons in Fig. 1 are downloaded from pixelsquid.com. This work was supported in part by the National Natural Science Foundation of China (Grant No.). In Urumqi station, The local surveying data is available through Zhang et al. (2013a), Zhang et al. (2013b), Zhang et al. (2015) and Zhang et al. (2019). The DOV data measured by the zenith tube is listed in Table. 3. The Digital Election Model (DEM) data in Fig. C.1 is from ASTER Global DEM dataset (Abrams et al., 2020) and is processed by the Global Mapper software.

References

Herrmann, H., & Bucksch, H. (2014). deviation (of the vertical). In Dictionary Geotechnical Engineering/Wörterbuch GeoTechnik (pp. 369–369). Springer Berlin Heidelberg. https://doi.org/10.1007/978-3-642-41714-6_41652

Barzaghi, R., Carrion, D., Pepe, M., & Prezioso, G. (2016). Computing the deflection of the vertical for improving aerial surveys: A comparison between EGM2008 and ITALGEO05 estimates. Sensors (Switzerland), 16(8). https://doi.org/10.3390/s16081168

Li, H., Fu, G. Y., & Li, Z. X. (2001). Plumb line deflection varied with time obtained by repeated gravimetry[J]. Acta Seismologica Sinica, 14(1):66-71.

Tanaka, Y., Okubo, S., Machida, M., et al. (2001). First detection of absolute gravity change caused by earthquake[J]. Geophysical Research Letters, 28(15):2979-2981.

Li, Z. X., & Li, H. (2009) Earthquake-related gravity field changes at Beijing-Tangshan gravimetric network during 1987–1998[J]. Studia Geophysica et Geodaetica, 53(2):p.185-197.

Ceylan, A. (2009). Determination of the deflection of vertical components via GPS and leveling measurement: A case study of a GPS test network in Konya, Turkey. Scientific Research & Essays„ 4(12):1438-1444.

Sun, F. H., Wu, X. P. & Zhang, C. D. (2005). Fast determination of the vertical deflection and its precision analysis of any point on the land and sea in China. Geomatics and Information Science of Wuhan University, 30(1): 42-46. (In Chinese)

Schuh, H., & Behrend, D. (2012). VLBI: A fascinating technique for geodesy and astrometry, J Geodyn., vol 61, pp 68-80.doi: 10.1016/j.jog.2012.07.007

Petrachenko, B., Niell, A., Behrend, D., Corey, B., Böhm, J., Charlot, P., et al. (2009). Design Aspects of the VLBI2010 System, Progress Report of the IVS VLBI2010 Committee. NASA/TM-2009-214180

Dawson, J., Sarti, P., Johnston, G. M., & Vittuari, L., (2007). Indirect approach to invariant point determination for SLR and VLBI systems: an assessment, J Geod., 81:433–441. DOI 10.1007/s00190-006-0125-x

Lösler, M., & Hennes, M., (2008). An innovative mathematical solution for a time-efficient IVS reference point determination, Measuring the changes, pp.12-15 (2008)

Lösler, M.. (2009). New mathematical model for reference point determination of an azimuth-elevation type radio telescope. J Surv Eng, 135 (4), pp. 131-135, 10.1061/(ASCE)SU.1943-5428.0000010

Kallio, U., & Poutanen, M., (2010). Can we really promise a mm-accuracy for the local ties on a geo-VLBI antenna. Geodesy for Planet Earth, Springer Berlin Heidelberg, pp. 35-42

Li, J., Zhang, J. W., & Guo, L., (2013). On the monitoring model of reference point of VLBI antenna, Science China Physics, Mechanics and Astronomy, 56(10): 1987-1994

Lösler, M., Haas, R., & Eschelbach, C., (2013). Automated and continual determination of radio telescope reference points with sub-mm accuracy: results from a campaign at the Onsala Space Observatory, J Geod., 87(8): 791-804

Ning, T., Haas, R., & Elgered, G., (2014). Determination of the Telescope Invariant Point and the Local Tie Vector at Onsala using GPS Measurements, IVS 2014 General Meeting Proceedings, pp.163-167

Lösler, M., (2008).Reference point determination with a new mathematical model at the 20 m VLBI radio telescope in Wettzell, Journal of Applied Geodesy 2 , pp. 233–238 DOI 10.1515/JAG.2008.026

Guiar, C. N., (1987). Lansing F L , Riggs R . Antenna Pointing Systematic Error Model Derivations. Telecommunications & Data Acquisition Progress Report, 1987, 88:36-46.

Zhao, Y. (2008) Research on modelling analysis and design of pointing errors for large radio telescope. Doctoral theses. Xidian University, 2008:2-10

Zhang, A. L., Xiong, F. W., & Zhu, W. Y. (2013). The Accuracy and Data Analysis of GPS Control Network at Nanshan Colocation Survey. Bulletin of Surveying and Mapping. 2013(12):4-7.(in Chinese)

Zhang, A. L., Xiong, F. W., & Zhu, W. Y. (2013).Analysis on GPS Observations in Collocation Survey at Xinjiang Astronomical Observatory. Journal of Geodesy and Geodynamics.2013, 33(5):129-132.(in Chinese)

Zhang, A. L., Xiong, F. W., & Zhu, W. Y. (2015). Co-Location Survey at Xinjiang Astronomical Observatory 25 m VLBI and GPS Station. Journal of Geodesy and Geodynamics, 2015, 35(4):680-683.(in Chinese)

Ma, X. H., Zhang. Z. B., Sun. Z. M., Mi, L. G., Lei, M., et al. (2021) A Small Scale Control Network Parameters Transformation Method for Surveying Deflection of the Vertical for Co-located Stations. Acta Astronomica Sinica. (accepted)

Krásná, H., Nickola, M., & Böhm, J. (2014). Axis Offset Estimation of VLBI Telescopes. International VLBI Service for Geodesy and Astrometry 2014 General Meeting Proceedings: "VGOS: The New VLBI Network", Eds. Dirk Behrend, Karen D. Baver, Kyla L. Armstrong, Science Press, Beijing, China, ISBN 978-7-03-042974-2, 2014, p. 339-343

Nilsson, T. (2015). Antenna axis offsets estimated in VLBI data analysis. In 22nd European VLBI for Geodesy and Astrometry Working Meeting Sao Miguel, Azores, May 17-21, 2015.

Kurdubov, S., & Skurikhina, E. (2010). Antenna Axis Offset Estimation from VLBI. In IVS 2010 General Meeting Proceedings.NASA/CP-2010-215864.

Koch, K. R., (2014) Robust estimations for the nonlinear Gauss Helmert model by the expectation maximization algorithm, J Geod. 88(3): 263-271 (2014)

Gipson, J., (1997).New reway, Calc/Solve User Guide.

Zhang, Z. B., Wang, G. L., Song, S. Z., Zhang, A.,& Wang, H. (2019). Modeling Azimuthal Steel-Track Deformation to Determine the Reference Point of Wheel-Track VLBI Antenna[J]. Geomatics and Information Science of Wuhan University, 44(10): 1498-1504.(in Chinese) doi: 10.13203/j.whugis20180050

Abrams, M., Crippen, R., & Fujisada, H. (2020). ASTER Global Digital Elevation Model (GDEM) and ASTER Global Water Body Dataset (ASTWBD). Remote Sensing, 12(7), 1156.